Eur. Phys. J. C 29, 313–323 (2003)
Digital Object Identifier (DOI) 10.1140/epjc/s2003-01235-0

THE EUROPEAN PHYSICAL JOURNAL C

Bhabha versus Møller scattering as a contact-interaction analyzer at a polarized Linear Collider

A. Pankov[1,2], N. Paver[1]

[1] Dipartimento di Fisica Teorica, Università di Trieste and Istituto Nazionale di Fisica Nucleare, Sezione di Trieste, Trieste, Italy
[2] Abdus Salam International Centre for Theoretical Physics, Trieste, Italy

Received: 15 October 2002 / Revised version: 28 April 2003 /
Published online: 18 June 2003 –

Abstract. We discuss electron–electron contact-interaction searches in the processes $e^+e^- \to e^+e^-$ and $e^-e^- \to e^-e^-$ at planned Linear Colliders run in the e^+e^- and e^-e^- modes with both beams longitudinally polarized. Our analysis is based on the measurement, for the two processes, of polarized differential cross sections, and allows one to simultaneously take into account the general set of electron contact-interaction couplings as independent, non-zero, parameters thus avoiding the simplifying choice of a model. We evaluate the corresponding model-independent constraints on the contact coupling constants, emphasizing the role of the available beam polarization and the complementarity, as far as the chirality of the constants is concerned, of the two processes in giving the best constraints.

1 Introduction

Contact-interaction (CI) Lagrangians provide a framework to account for the phenomenological effects of non-standard dynamics characterized by extremely large intrinsic mass scales Λ, at the "low" energies $\sqrt{s} \ll \Lambda$ attainable at current particle accelerators. One of the historical motivations for considering such a framework is the fact that "low energy" manifestations of quark and lepton substructure would occur *via* four-fermion quark and lepton contact interactions, induced by exchanges of quite heavy sub-constituent bound states with mass of the order of Λ. Indeed, in the spirit of the "effective interactions", this concept can be used more generally, to parameterize non-standard, very heavy particle exchanges in reactions among quarks and leptons, in the form of "low energy" expansions of the relevant amplitudes at the leading order in $\sqrt{s}/\Lambda$. Since the above mentioned exchanged heavy particles, with mass $M \gg M_{W,Z}$, could not be directly produced at the collider energy $\sqrt{s}$, the underlying non-standard dynamics could experimentally manifest itself only indirectly, by deviations of the measured observables from the standard model (SM) predictions. If such deviations were effectively observed to a given significance level, one could try to gain numerical information on the parameters (masses and coupling constants) of non-standard models and, eventually, select the viable ones [1,2]. In the case where, instead, no deviation from the SM predictions is observed within the experimental accuracy, one can set numerical bounds or constraints on the parameters characterizing the new interactions, and determine the discovery reach of planned high energy colliders. Clearly, also this kind of information should be phenomenologically useful in model applications.

The explicit form of the contact-interaction Lagrangian depends on the kind of external particles participating in the considered reaction. For the Bhabha scattering process of interest here:

$$e^+ + e^- \to e^+ + e^-, \tag{1}$$

as well as for Møller scattering:

$$e^- + e^- \to e^- + e^-, \tag{2}$$

we consider the four-fermion contact-interaction Lagrangian [3]

$$\mathcal{L}_{\rm CI} = \frac{1}{1+\delta_{ef}} \sum_{i,j} g^2_{\rm eff}\, \epsilon_{ij} \left(\bar{e}_i \gamma_\mu e_i\right) \left(\bar{f}_j \gamma^\mu f_j\right). \tag{3}$$

In (3) $i,j = {\rm L,R}$ denote left- or right-handed fermion helicities, $\delta_{ef} = 1$ for processes (1) and (2), and the same Lagrangian, with $\delta_{ef} = 0$, is relevant to the annihilation processes

$$e^+ + e^- \to l^+ + l^-, \tag{4}$$

with $l = \mu, \tau$. The CI coupling constants in (3) are parameterized in terms of the corresponding mass scales by $\epsilon_{ij} = \eta_{ij}/\Lambda^2_{ij}$ and, according to the previous remarks concerning compositeness, one assumes $g^2_{\rm eff} = 4\pi$. Also, by convention, one takes $|\eta_{ij}| = 1$ or $\eta_{ij} = 0$, leaving the energy scales Λ_{ij} as free, a priori independent, parameters. The explicit $SU(3) \times SU(2) \times U(1)$ symmetry of the helicity conserving four-fermion lepton contact interaction (3)

reflects that the new dynamics are active well-beyond the electroweak scale. Furthermore, (3) represents the lowest-dimensional operator, $D = 6$ being the minimum, and higher-dimensional operators, suppressed by higher powers of s/Λ^2, are supposed to be negligible.

As anticipated, we will study the effects of the interaction (3) in processes (1) and (2) at an e^+e^- Linear Collider with c.m. energy $\sqrt{s} = 0.5\,\text{TeV}$ and polarized electron and positron beams [4,5]. Indeed, the possibility of studying e^-e^- initiated processes, in particular new physics, at such a facility by turning the positron beam into an electron one, has been recently considered with interest [6]. Therefore, it should be useful to evaluate, and compare, the sensitivities to the CI coupling constants that can be obtained from the measurements of processes (1) and (2).

Clearly, from current lower bounds on Λs obtained at LEP [7,8], of the order of 10–15 TeV depending on the specific models chosen to fit the data, we can assume $s \ll \Lambda^2$, so that the relative size of the deviations from the SM induced by (3) is expected to be of order $s/\alpha\Lambda^2$, with α the SM coupling (essentially, the fine structure constant), and therefore it is expected to be quite small[1]. Consequently, very high collider energies and luminosities are required to attain a significant sensitivity on these effects.

We notice that for the case of the Bhabha process (1), (3) envisages the existence of six independent CI models, each one contributing to individual helicity amplitudes or combinations of them, with a priori free, and non-vanishing, coefficients (basically, $\epsilon_{\rm LL}, \epsilon_{\rm RR}$ and $\epsilon_{\rm LR} = \epsilon_{\rm RL}$ combined with the $\pm$ signs). The same is true for the Møller process (2)[2]. Correspondingly, in principle, a model-independent analysis of the data should account for the situation where the full equation (3) is included in the expression for the cross section. Potentially, in this case, the different CI couplings may interfere and such interference could substantially weaken the bounds because, although the different helicity amplitudes by themselves do not interfere, the deviations from the SM could be positive for one helicity amplitude and negative for another, so that accidental cancellations might occur in the sought for deviations of the relevant observables from the SM predictions.

The analysis of processes (1) and (2) proposed here relies on the initial beams longitudinal polarization envisaged at the planned Linear Colliders. The polarization can be exploited to extract the values of the individual helicity cross sections from suitable combinations of measurable polarized cross sections and, consequently, to disentangle the effects of the corresponding CI constants ϵ_{ij}; see, e.g., [11]. Therefore, all CI couplings of (3) are simultaneously included as independent, non-vanishing, free parameters and, yet, separate constraints (or exclusion regions) on their values can be obtained, free from potential weakening due to accidental cancellations. In this sense, the procedure should be considered as model independent. We will also make a comparison of the results with those obtained from the simplest, model-dependent, procedure of assuming non-zero values for only one of the couplings (or one specific combination of them) at a time, with all others set to zero.

Specifically, in Sect. 2 we introduce the polarized observables for the Bhabha and the Møller processes, (1) and (2), and discuss the sensitivities of the different angular ranges to the CI couplings in the two cases. In Sect. 3 we perform the numerical analysis, based on a χ^2 procedure, to derive the constraints on the CI couplings and establish the attainable reach on the mass scales Λ_{ij} as a function of the integrated luminosity. Section 4 contains some conclusive remarks, in particular a comparison of the results from the two processes.

2 Polarized observables

2.1 Bhabha scattering

With P^- and P^+ the longitudinal polarization of the electron and positron beams, respectively, and θ the angle between the incoming and the outgoing electrons in the c.m. frame, the differential cross section of process (1) at lowest order, including γ and Z exchanges both in the s and t channels and the contact interaction (3), can be written in the following form [12–16]:

$$\begin{aligned}\frac{\mathrm{d}\sigma(P^-,P^+)}{\mathrm{d}\cos\theta} &= \frac{(1+P^-)\,(1-P^+)}{4}\,\frac{\mathrm{d}\sigma_{\rm R}}{\mathrm{d}\cos\theta} \\ &+ \frac{(1-P^-)\,(1+P^+)}{4}\,\frac{\mathrm{d}\sigma_{\rm L}}{\mathrm{d}\cos\theta} \\ &+ \frac{(1+P^-)(1+P^+)}{4}\,\frac{\mathrm{d}\sigma_{{\rm RL},t}}{\mathrm{d}\cos\theta} \\ &+ \frac{(1-P^-)(1-P^+)}{4}\,\frac{\mathrm{d}\sigma_{{\rm LR},t}}{\mathrm{d}\cos\theta}. \end{aligned} \tag{5}$$

In (5):

$$\begin{aligned}\frac{\mathrm{d}\sigma_{\rm L}}{\mathrm{d}\cos\theta} &= \frac{\mathrm{d}\sigma_{\rm LL}}{\mathrm{d}\cos\theta} + \frac{\mathrm{d}\sigma_{{\rm LR},s}}{\mathrm{d}\cos\theta}, \\ \frac{\mathrm{d}\sigma_{\rm R}}{\mathrm{d}\cos\theta} &= \frac{\mathrm{d}\sigma_{\rm RR}}{\mathrm{d}\cos\theta} + \frac{\mathrm{d}\sigma_{{\rm RL},s}}{\mathrm{d}\cos\theta}, \end{aligned} \tag{6}$$

with

$$\begin{aligned}\frac{\mathrm{d}\sigma_{\rm LL}}{\mathrm{d}\cos\theta} &= \frac{2\pi\alpha^2}{s}\left|A_{\rm LL}\right|^2, \\ \frac{\mathrm{d}\sigma_{\rm RR}}{\mathrm{d}\cos\theta} &= \frac{2\pi\alpha^2}{s}\left|A_{\rm RR}\right|^2, \\ \frac{\mathrm{d}\sigma_{{\rm LR},t}}{\mathrm{d}\cos\theta} &= \frac{\mathrm{d}\sigma_{{\rm RL},t}}{\mathrm{d}\cos\theta} = \frac{2\pi\alpha^2}{s}\left|A_{{\rm LR},t}\right|^2, \\ \frac{\mathrm{d}\sigma_{{\rm LR},s}}{\mathrm{d}\cos\theta} &= \frac{\mathrm{d}\sigma_{{\rm RL},s}}{\mathrm{d}\cos\theta} = \frac{2\pi\alpha^2}{s}\left|A_{{\rm LR},s}\right|^2, \end{aligned} \tag{7}$$

and

$$A_{\rm RR} = \frac{u}{s}\left[1 + \frac{s}{t} + g_{\rm R}^2\,\left(\chi_Z(s) + \frac{s}{t}\,\chi_Z(t)\right) + 2\frac{s}{\alpha}\,\epsilon_{\rm RR}\right],$$

[1] For bounds from different kinds of processes, in particular on contact couplings to quarks, see, e.g., [9,10]

[2] In general, apart from the $\pm$ possibility, for $e^+e^- \to \bar{f}f$ with $f \neq e$ there are four independent CI couplings, so that in the present case of processes (1) and (2) there is one free parameter less

$$A_{\rm LL} = \frac{u}{s}\left[1+\frac{s}{t}+g_{\rm L}^2\left(\chi_Z(s)+\frac{s}{t}\chi_Z(t)\right)+2\frac{s}{\alpha}\epsilon_{\rm LL}\right],$$
$$A_{{\rm LR},s} = \frac{t}{s}\left[1+g_{\rm R}\,g_{\rm L}\,\chi_Z(s)+\frac{s}{\alpha}\epsilon_{\rm LR}\right],$$
$$A_{{\rm LR},t} = \frac{s}{t}\left[1+g_{\rm R}\,g_{\rm L}\chi_Z(t)+\frac{t}{\alpha}\epsilon_{\rm LR}\right]. \quad (8)$$

Here α is the fine structure constant; $t=-s(1-\cos\theta)/2$, $u=-s(1+\cos\theta)/2$ and $\chi_Z(s)=s/(s-M_Z^2+{\rm i}M_Z\Gamma_Z)$ and $\chi_Z(t)=t/(t-M_Z^2)$ represent the Z propagator in the s and t channels, respectively, with M_Z and Γ_Z the mass and width of the Z; $g_{\rm R}=\tan\theta_{\rm W}$, $g_{\rm L}=-\cot 2\,\theta_{\rm W}$ are the SM right- and left-handed electron couplings of the Z, with $\theta_{\rm W}$ the electroweak mixing angle. Furthermore, notice that P^- (P^+) are the degrees of initial e^- (e^+) longitudinal polarization, each one oriented along the respective momentum, and we are using the right-handed helicity basis so that, for example, $P^-,P^+=-1$ indicates "pure" (100%) left-handed e^- and e^+.

With both beams polarized, the polarization of each beam can be changed on a pulse by pulse basis. This would allow the separate measurement of the polarized cross sections to be made for each of the three polarization configurations $++$, $+-$ and $-+$, corresponding to the sets of beam polarizations $(P^-,P^+)=(P_1,P_2)$, $(P_1,-P_2)$ and $(-P_1,P_2)$, respectively, with $P_{1,2}>0$. Specifically, from (5), with the simplifying notation ${\rm d}\sigma\equiv{\rm d}\sigma/{\rm d}\cos\theta$:

$$\begin{aligned}
{\rm d}\sigma_{++} &= \frac{(1+P_1)(1-P_2)}{4}\,{\rm d}\sigma_{\rm R} \\
&\quad+\frac{(1-P_1)(1+P_2)}{4}\,{\rm d}\sigma_{\rm L}+\frac{1+P_1P_2}{2}\,{\rm d}\sigma_{{\rm LR},t},\\
{\rm d}\sigma_{+-} &= \frac{(1+P_1)(1+P_2)}{4}\,{\rm d}\sigma_{\rm R} \\
&\quad+\frac{(1-P_1)(1-P_2)}{4}\,{\rm d}\sigma_{\rm L}+\frac{1-P_1P_2}{2}\,{\rm d}\sigma_{{\rm LR},t},\\
{\rm d}\sigma_{-+} &= \frac{(1-P_1)(1-P_2)}{4}\,{\rm d}\sigma_{\rm R} \\
&\quad+\frac{(1+P_1)(1+P_2)}{4}\,{\rm d}\sigma_{\rm L}+\frac{1-P_1P_2}{2}\,{\rm d}\sigma_{{\rm LR},t}.
\end{aligned} \quad (9)$$

To extract from the measured polarized cross sections the values of ${\rm d}\sigma_{\rm R}$, ${\rm d}\sigma_{\rm L}$ and ${\rm d}\sigma_{{\rm LR},t}$, that carry the information on the CI couplings, one has to invert the system of (9). The solution reads

$$\begin{aligned}
{\rm d}\sigma_{\rm R} &= \frac{(1+P_2)^2}{2P_2(P_1+P_2)}\,{\rm d}\sigma_{+-}+\frac{(1-P_1)^2}{2P_1(P_1+P_2)}\,{\rm d}\sigma_{-+}\\
&\quad-\frac{1-P_1P_2}{2P_1P_2}\,{\rm d}\sigma_{++},\\
{\rm d}\sigma_{\rm L} &= \frac{(1-P_2)^2}{2P_2(P_1+P_2)}\,{\rm d}\sigma_{+-}+\frac{(1+P_1)^2}{2P_1(P_1+P_2)}\,{\rm d}\sigma_{-+}\\
&\quad-\frac{1-P_1P_2}{2P_1P_2}\,{\rm d}\sigma_{++},\\
{\rm d}\sigma_{{\rm LR},t} &= -\frac{1-P_2^2}{2P_2(P_1+P_2)}\,{\rm d}\sigma_{+-}-\frac{1-P_1^2}{2P_1(P_1+P_2)}\,{\rm d}\sigma_{-+}\\
&\quad+\frac{1+P_1P_2}{2P_1P_2}\,{\rm d}\sigma_{++}.
\end{aligned} \quad (10)$$

As one can see from (6)–(8), $\sigma_{{\rm LR},t}$ depends on a single contact-interaction parameter ($\epsilon_{\rm LR}$), while $\sigma_{\rm R}$ and $\sigma_{\rm L}$ depend on pairs of parameters, ($\epsilon_{\rm RR}$, $\epsilon_{\rm LR}$) and ($\epsilon_{\rm LL}$, $\epsilon_{\rm LR}$), respectively. Therefore, the derivation of the model-independent constraints on the CI couplings requires the combination of all polarized cross sections as in (10). In this regard, to emphasize the role of polarization, one can easily notice from (5)–(8) that in the unpolarized case $P_1=P_2=0$, the interference of the $\epsilon_{\rm LR}$ term with the SM amplitude in $A_{{\rm LR},s}$ and $A_{{\rm LR},t}$ has opposite signs, leading to a partial cancellation for $-t\sim s$. From the explicit expression of t given below (8), such a cancellation occurs in the region of large scattering angle θ. Consequently, as briefly anticipated in Sect. 1, one can expect the unpolarized cross section to have reduced sensitivity to $\epsilon_{\rm LR}$. Conversely, $\epsilon_{\rm LR}$ is *directly* accessible from ${\rm d}\sigma_{{\rm LR},t}$, via polarized cross sections as in (10). Also, considering that numerically $g_{\rm L}^2\cong g_{\rm R}^2$, the parameters $\epsilon_{\rm LL}$ and $\epsilon_{\rm RR}$ contribute to the unpolarized cross section through $A_{\rm RR}$ and $A_{\rm LL}$ with equal coefficients, so that, in general, only correlations of the form $|\epsilon_{\rm LL}+\epsilon_{\rm RR}|<{\rm const}$, and not finite allowed regions, could be derived in the unpolarized case. Since we have three unknown contact couplings, the three spin combinations of (9) are sufficient to determine them. In principle, one could have chosen alternative spin configurations, including for instance ${\rm d}\sigma_{--}$. Numerically, we find that the configurations chosen in (9) show a slightly better sensitivity to $\Lambda_{\rm LR}$.

To make contact to the experimental situation we take $P_1=0.8$ and $P_2=0.6$, and impose a cut in the forward and backward directions. Specifically, we consider the cut angular range $|\cos\theta|<0.9$ and divide it into nine equal-size bins of width $\Delta z=0.2$ ($z\equiv\cos\theta$). We also introduce the experimental efficiency, ϵ, for detecting the final e^+e^- pair and $\epsilon=99\%$ is assumed.

We then define the three, directly measurable, event rates integrated over each bin:

$$N_{++},\quad N_{+-},\quad N_{-+}, \quad (11)$$

and ($\alpha\beta=++$, etc.):

$$N_{\alpha\beta}^{\rm bin}=\frac{1}{3}\mathcal{L}_{\rm int}(e^+e^-)\,\epsilon\int_{\rm bin}({\rm d}\sigma_{\alpha\beta}/{\rm d}z){\rm d}z. \quad (12)$$

In (12), $\mathcal{L}_{\rm int}=\int\mathcal{L}{\rm d}t$ is the time-integrated luminosity over one "running year" of $10^7\,s$, and is assumed to be equally divided among the three combinations of electron and positron beam polarizations defined in (9). Clearly, the numerical results on the individual contact couplings would be different from the ones obtained here in the case where the luminosity at the future Linear Collider would not be equally shared among the three configurations, and should be recalculated according to the actual running times. For example, from (10) one can easily see that less running time to the combination $(++)$ would mostly affect the bounds on $\Lambda_{\rm LR}$ and the same is true for the other polarization combinations.

In Fig. 1, the bin-integrated angular distributions of $N_{++}^{\rm bin}$ and $N_{+-}^{\rm bin}$ in the SM at $\sqrt{s}=500\,{\rm GeV}$, $\mathcal{L}_{\rm int}=$

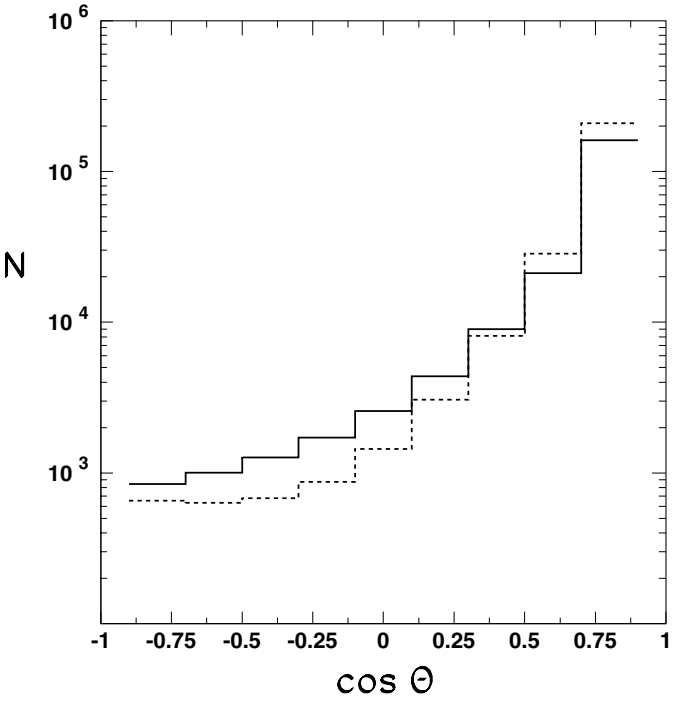

Fig. 1. Bin-integrated angular distributions of $N^{\rm bin}_{++}$ (solid line) and $N^{\rm bin}_{+-}$ (dashed line), (12), in the SM at $\sqrt{s} = 500\,\text{GeV}$, $\mathcal{L}_{\rm int}(e^+e^-) = 50\,\text{fb}^{-1}$, $|P^-| = 0.8$ and $|P^+| = 0.6$

$50\,\text{fb}^{-1}$, and longitudinal polarizations $|P^-| = 0.8$ and $|P^+| = 0.6$, are presented as histograms. Here, the SM cross sections have been evaluated by means of the effective Born approximation [17,18]. The typical forward peak, dominated by the t-channel photon pole, dramatically shows up, and determines a really large statistics available in the region of small t. The $\cos\theta$ distribution for the remaining polarization configuration $N^{\rm bin}_{-+}$ in (9) is similar to $N^{\rm bin}_{+-}$ due to $|g_{\rm L}| \simeq |g_{\rm R}|$ in the SM, and would be practically indistinguishable in Fig. 1. Therefore, we do not represent it here.

The next step is to define the relative deviations of the polarized cross sections from the SM predictions, due to the contact interaction. In general, for such deviations, we use the notation:

$$\Delta(\mathcal{O}) = \frac{\mathcal{O}(\text{SM} + \text{CI}) - \mathcal{O}(\text{SM})}{\mathcal{O}(\text{SM})}, \tag{13}$$

where $\mathcal{O} = \sigma_{\rm R}$, $\sigma_{\rm L}$ and $\sigma_{{\rm LR},t}$. To get an illustration of the effect of the contact interactions on the observables (10) under consideration, we show in Fig. 2a,b,c the angular distributions of the relative deviations of $\mathrm{d}\sigma_{\rm R}$ and $\mathrm{d}\sigma_{{\rm LR},t}$, taking as examples the values of $\mathcal{L}_{\rm int}$ and Λ_{ij} indicated in the caption. The SM predictions are evaluated in the same effective Born approximation as in Fig. 1. The deviations $\Delta(\mathcal{O})$ are then compared to the expected statistical relative uncertainties, represented by the vertical bars. Figure 2a,c show that $\mathrm{d}\sigma_{\rm R}$ is sensitive to the contact interaction $\epsilon_{\rm RR}$ in the forward region, where the ratio of the "signal" to the statistical uncertainty substantially increases, while it is sensitive to $\epsilon_{\rm LR}$ in the backward direction. Also, it qualitatively indicates that, for the chosen values of the c.m. energy $\sqrt{s}$ and $\mathcal{L}_{\rm int}$, the reach on $\Lambda_{\rm RR}$ will be substantially larger than 30 TeV. Conversely, Fig. 2b shows that the sensitivity of $\mathrm{d}\sigma_{{\rm LR},t}$ is almost independent on the chosen kinematical range in $\cos\theta$, leading to a really high sensitivity of this observable to $\epsilon_{\rm LR}$, and to a corresponding reach on $\Lambda_{\rm LR}$ potentially larger than 50 TeV. The corresponding behavior of the statistical significances, defined as the ratio between the deviation from the SM and the statistical uncertainty for each bin, $\mathcal{S}(\mathcal{O}) = \Delta(\mathcal{O})/\delta\mathcal{O}$ with $\delta\mathcal{O}$ the expected statistical relative uncertainty, are shown in Fig. 3a,b. One can notice from (8) that the statistical significance $\mathcal{S}$ goes to zero in the limit $\theta \to 0$. This is not evident from Fig. 3a,b due to the limited kinematical region $|\cos\theta| < 0.9$ taken in our analysis.

2.2 Møller scattering

With P_1^- and P_2^- the longitudinal polarization of the electron beams, the differential cross section of process (2) can be written in the following form [19–21][3]:

$$\begin{aligned}\frac{\mathrm{d}\sigma(P_1^-, P_2^-)}{\mathrm{d}\cos\theta} &= \frac{(1+P_1^-)\,(1+P_2^-)}{4}\,\frac{\mathrm{d}\sigma_{\rm RR}}{\mathrm{d}\cos\theta} \\ &+ \frac{(1-P_1^-)\,(1-P_2^-)}{4}\,\frac{\mathrm{d}\sigma_{\rm LL}}{\mathrm{d}\cos\theta} \\ &+ \frac{1-P_1^-P_2^-}{2}\,\left(\frac{\mathrm{d}\sigma_{{\rm LR},t}}{\mathrm{d}\cos\theta} + \frac{\mathrm{d}\sigma_{{\rm LR},u}}{\mathrm{d}\cos\theta}\right).\end{aligned} \tag{14}$$

In (14):

$$\begin{aligned}\frac{\mathrm{d}\sigma_{\rm RR}}{\mathrm{d}\cos\theta} &= \frac{\pi\alpha^2}{s}\big|A_{\rm RR}\big|^2, \quad \frac{\mathrm{d}\sigma_{\rm LL}}{\mathrm{d}\cos\theta} = \frac{\pi\alpha^2}{s}\big|A_{\rm LL}\big|^2, \\ \frac{\mathrm{d}\sigma_{{\rm LR},u}}{\mathrm{d}\cos\theta} &= \frac{\pi\alpha^2}{s}\big|A_{{\rm LR},u}\big|^2, \quad \frac{\mathrm{d}\sigma_{{\rm LR},t}}{\mathrm{d}\cos\theta} = \frac{\pi\alpha^2}{s}\big|A_{{\rm LR},t}\big|^2,\end{aligned} \tag{15}$$

and

$$\begin{aligned}A_{\rm RR} &= \frac{s}{t}\left[1 + \frac{t}{u} + g_{\rm R}^2\,\left(\chi_Z(t) + \frac{t}{u}\,\chi_Z(u)\right) + 2\frac{t}{\alpha}\,\epsilon_{\rm RR}\right], \\ A_{\rm LL} &= \frac{s}{t}\left[1 + \frac{t}{u} + g_{\rm L}^2\,\left(\chi_Z(t) + \frac{t}{u}\,\chi_Z(u)\right) + 2\frac{t}{\alpha}\,\epsilon_{\rm LL}\right], \\ A_{{\rm LR},u} &= \frac{t}{u}\left[1 + g_{\rm R}\,g_{\rm L}\,\chi_Z(u) + \frac{u}{\alpha}\,\epsilon_{\rm LR}\right], \\ A_{{\rm LR},t} &= \frac{u}{t}\left[1 + g_{\rm R}\,g_{\rm L}\,\chi_Z(t) + \frac{t}{\alpha}\,\epsilon_{\rm LR}\right],\end{aligned} \tag{16}$$

where $\chi_Z(u) = u/(u - M_Z^2)$. Notice that the amplitudes A_{ij} are now functions of t and u instead of t and s as in the case of Bhabha scattering.

As for the previous process, with both beams polarized the polarization of each electron beam can be changed

[3] In the case of Møller scattering one can find for the cross section results similar to Bhabha scattering, that can be obtained by crossing symmetry except for the overall normalization factor 1/2 related to identical particles

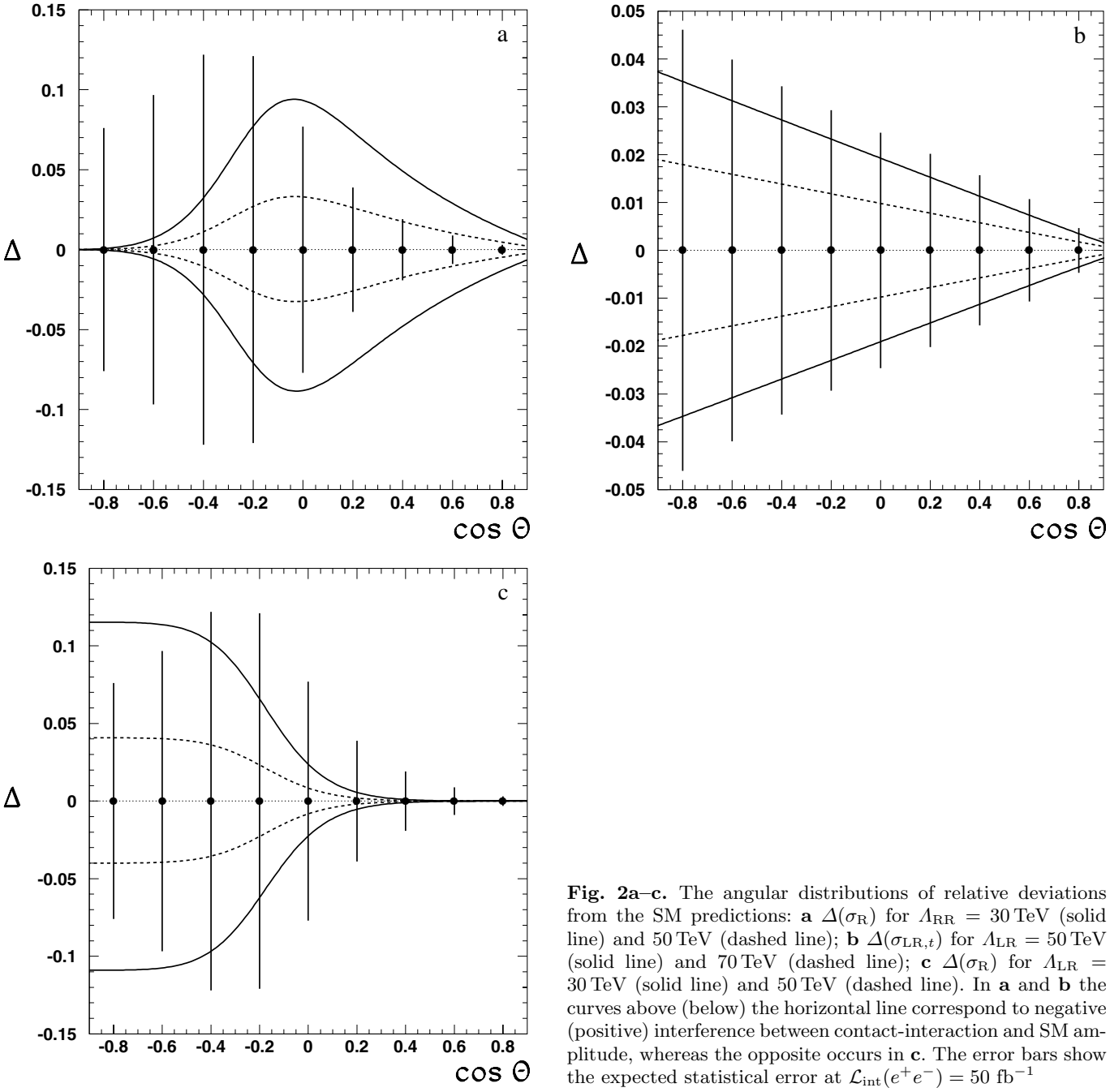

Fig. 2a–c. The angular distributions of relative deviations from the SM predictions: **a** $\Delta(\sigma_{\rm R})$ for $\Lambda_{\rm RR} = 30\,{\rm TeV}$ (solid line) and 50 TeV (dashed line); **b** $\Delta(\sigma_{{\rm LR},t})$ for $\Lambda_{\rm LR} = 50\,{\rm TeV}$ (solid line) and 70 TeV (dashed line); **c** $\Delta(\sigma_{\rm R})$ for $\Lambda_{\rm LR} = 30\,{\rm TeV}$ (solid line) and 50 TeV (dashed line). In **a** and **b** the curves above (below) the horizontal line correspond to negative (positive) interference between contact-interaction and SM amplitude, whereas the opposite occurs in **c**. The error bars show the expected statistical error at $\mathcal{L}_{\rm int}(e^+e^-) = 50\ {\rm fb}^{-1}$

on a pulse by pulse basis. This would allow the separate measurement to be made of the polarized cross sections for each of the three polarization configurations $++$, $--$ and $+-$, corresponding to the sets of beam polarizations $(P_1^-, P_2^-) = (P_1, P_2)$, $(-P_1, -P_2)$ and $(P_1, -P_2)$, respectively, with $P_{1,2} > 0$. From (14)

$$\begin{aligned}
{\rm d}\sigma_{++} &= \frac{(1+P_1)(1+P_2)}{4}\,{\rm d}\sigma_{\rm RR} \\
&\quad + \frac{(1-P_1)(1-P_2)}{4}\,{\rm d}\sigma_{\rm LL} + \frac{1-P_1P_2}{2}\,{\rm d}\sigma_{\rm LR}, \\
{\rm d}\sigma_{--} &= \frac{(1-P_1)(1-P_2)}{4}\,{\rm d}\sigma_{\rm RR} \\
&\quad + \frac{(1+P_1)(1+P_2)}{4}\,{\rm d}\sigma_{\rm LL} + \frac{1-P_1P_2}{2}\,{\rm d}\sigma_{\rm LR}, \\
{\rm d}\sigma_{+-} &= \frac{(1+P_1)(1-P_2)}{4}\,{\rm d}\sigma_{\rm RR} \\
&\quad + \frac{(1-P_1)(1+P_2)}{4}\,{\rm d}\sigma_{\rm LL} + \frac{1+P_1P_2}{2}\,{\rm d}\sigma_{\rm LR}.
\end{aligned} \tag{17}$$

To extract from the measured polarized cross sections the values of ${\rm d}\sigma_{\rm RR}$, ${\rm d}\sigma_{\rm LL}$ and ${\rm d}\sigma_{\rm LR}$, that carry the information on individual CI couplings, one has to invert the system of (17). The solution reads

$$\begin{aligned}
{\rm d}\sigma_{\rm RR} &= \frac{(1+P_2)^2}{2P_2(P_1+P_2)}\,{\rm d}\sigma_{++} + \frac{(1-P_1)^2}{2P_1(P_1+P_2)}\,{\rm d}\sigma_{--} \\
&\quad - \frac{1-P_1^2}{2P_1P_2}\,{\rm d}\sigma_{\rm LR} - \frac{1-P_2^2}{2P_1P_2}\,{\rm d}\sigma_{\rm LL}, \\
{\rm d}\sigma_{\rm LL} &= \frac{(1+P_1)^2}{2P_1(P_1+P_2)}\,{\rm d}\sigma_{+-} + \frac{(1-P_2)^2}{2P_2(P_1+P_2)}\,{\rm d}\sigma_{-+} \\
&\quad - \frac{1-P_1^2}{2P_1P_2}\,{\rm d}\sigma_{\rm LR} - \frac{1-P_2^2}{2P_1P_2}\,{\rm d}\sigma_{\rm RR}, \\
{\rm d}\sigma_{\rm LR} &= \frac{(1+P_1)(1+P_2)}{4P_1P_2}\,{\rm d}\sigma_{+-} + \frac{(1-P_1)(1-P_2)}{4P_1P_2}\,{\rm d}\sigma_{-+} \\
&\quad - \frac{1-P_1^2}{4P_1P_2}\,{\rm d}\sigma_{\rm LL} - \frac{1-P_2^2}{4P_1P_2}\,{\rm d}\sigma_{\rm RR}.
\end{aligned} \tag{18}$$

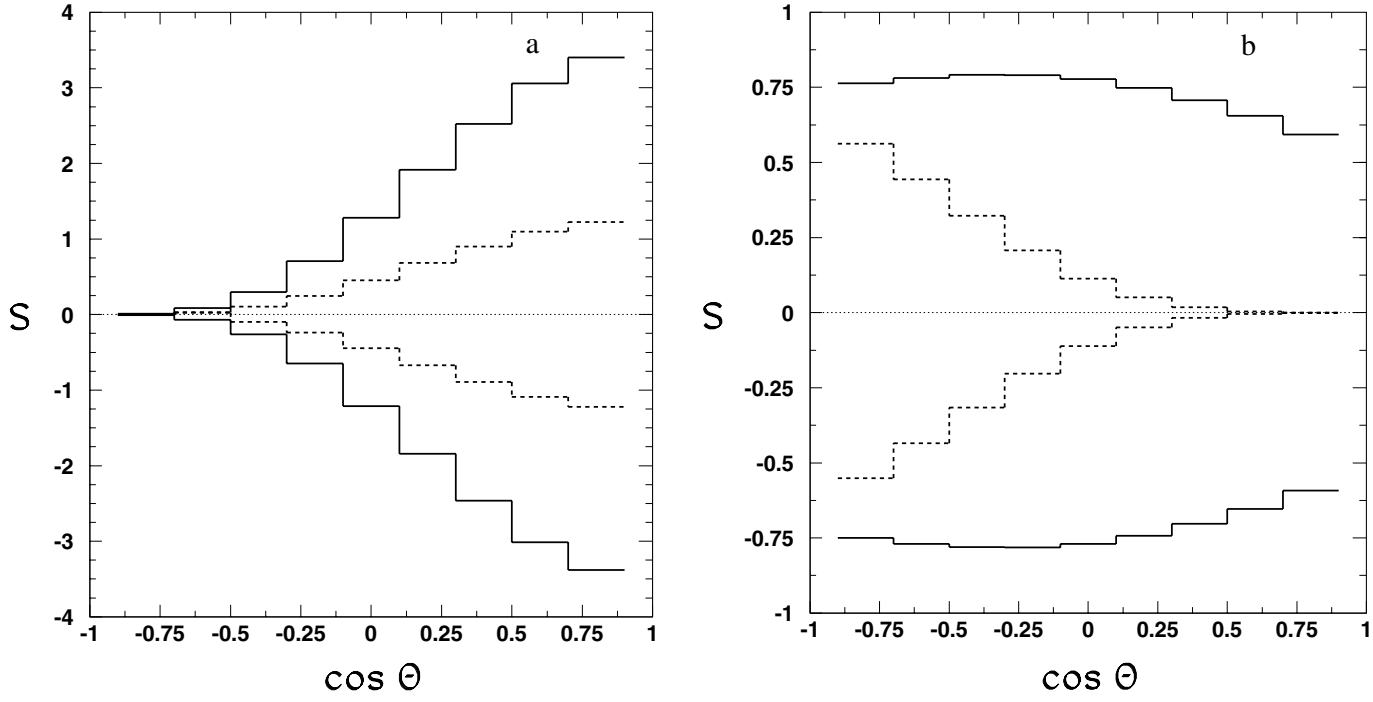

Fig. 3. a Statistical significance $\mathcal{S}(\sigma_R)$ as a function of $\cos\theta$ at $\Lambda_{\rm RR} = 30\,\text{TeV}$ (solid line) and 50 TeV (dashed line); **b** Statistical significance $\mathcal{S}(\sigma_R)$ (dashed line) and $\mathcal{S}(\sigma_{{\rm LR},t})$ (solid line) as a function of $\cos\theta$ at $\Lambda_{\rm LR} = 50\,\text{TeV}$. Here: $\sqrt{s} = 500\,\text{GeV}$, $\mathcal{L}_{\rm int}(e^+e^-) = 50\,\text{fb}^{-1}$, $|P^-| = 0.8$ and $|P^+| = 0.6$

$$
\begin{aligned}
&- \frac{1-P_1P_2}{2P_1P_2}\,\mathrm{d}\sigma_{+-},\\
\mathrm{d}\sigma_{\rm LL} &= \frac{(1-P_2)^2}{2P_2(P_1+P_2)}\,\mathrm{d}\sigma_{++} + \frac{(1+P_1)^2}{2P_1(P_1+P_2)}\,\mathrm{d}\sigma_{--}\\
&- \frac{1-P_1P_2}{2P_1P_2}\,\mathrm{d}\sigma_{+-},\\
\mathrm{d}\sigma_{\rm LR} &= -\frac{1-P_2^2}{2P_2(P_1+P_2)}\,\mathrm{d}\sigma_{++} - \frac{1-P_1^2}{2P_1(P_1+P_2)}\,\mathrm{d}\sigma_{--}\\
&+ \frac{1+P_1P_2}{2P_1P_2}\,\mathrm{d}\sigma_{+-}. \qquad (18)
\end{aligned}
$$

As one can see from (15) and (16), contrary to the case of Bhabha scattering, each of the cross sections $\sigma_{\rm RR}$, $\sigma_{\rm LL}$ *and* $\sigma_{\rm LR}$ depend on an individual contact-interaction parameter, so that full disentanglement of the various couplings (hence the derivation of model-independent constraints) is directly obtained by electron beams polarization in the Møller process.

Similar to Sect. 2.1, see (11) and (12), we define measurable event rates integrated over each bin in $z = \cos\theta$:

$$N_{++}, \quad N_{--}, \quad N_{+-}, \qquad (19)$$

and ($\alpha\beta = ++$, etc.):

$$N^{\rm bin}_{\alpha\beta} = \frac{1}{3}\mathcal{L}_{\rm int}(e^-e^-)\,\epsilon \int_{\rm bin} (\mathrm{d}\sigma_{\alpha\beta}/\mathrm{d}z)\mathrm{d}z. \qquad (20)$$

In (20), $\mathcal{L}_{\rm int}$ is the time-integrated luminosity in the e^-e^- mode of the Linear Collider, and is assumed to be equally divided among the three combinations of electron beams polarizations defined in (17). Figure 4 is the analogue of Fig. 1 for Bhabha scattering and represents the bin-integrated angular distributions of $N^{\rm bin}_{++}$ and $N^{\rm bin}_{+-}$ in the SM, calculated by means of the effective Born approximation, for the c.m. energy $\sqrt{s} = 500\,\text{GeV}$. To account for the lower luminosity in the e^-e^- mode due to anti-pinching in the interaction region [6,22], we assume in the example of Fig. 4 $\mathcal{L}_{\rm int}(e^-e^-) \simeq \frac{1}{3}\mathcal{L}_{\rm int}(e^+e^-)$ as expected for the NLC [5]. Also, as regards the longitudinal polarization of electrons, we take the symmetric configuration $|P_1^-| = |P_2^-| = 0.8$.

One should notice, in this case of Møller scattering, the peaks in the forward and backward directions, dominated by the t and u photon poles leading to high statistics in those kinematical regions, and the dip at 90°. The $\cos\theta$ distribution for $N^{\rm bin}_{--}$ has similar features.

Relative deviations of $\sigma_{\rm RR}$, $\sigma_{\rm LL}$ and $\sigma_{\rm LR}$ from the SM model due to the contact interactions can be defined in analogy to (13). In Fig. 5 we show the angular distribution of the deviations $\Delta(\sigma_{\rm RR})$ and $\Delta(\sigma_{\rm LR})$, for the values of $\mathcal{L}_{\rm int}(e^-e^-)$ and Λ_{ij} indicated in the caption, and with the SM predictions evaluated in the same effective Born approximation used in Fig. 4. Such deviations are compared to the expected statistical uncertainties represented by the vertical bars. The indication of Fig. 5, the analogue of Fig. 2 for Bhabha scattering, is that, in Møller scattering, the sensitivity of $\sigma_{\rm RR}$ to the related contact parameter $\epsilon_{\rm RR}$ is almost flat in $\cos\theta$ leading to high sensitivity to $\epsilon_{\rm RR}$ (the same occurs for $\sigma_{\rm LL}$ and $\epsilon_{\rm LL}$). Conversely, maximal sensitivity to $\epsilon_{\rm LR}$ is obtained in the forward and backward regions where the expected statistical uncertainties

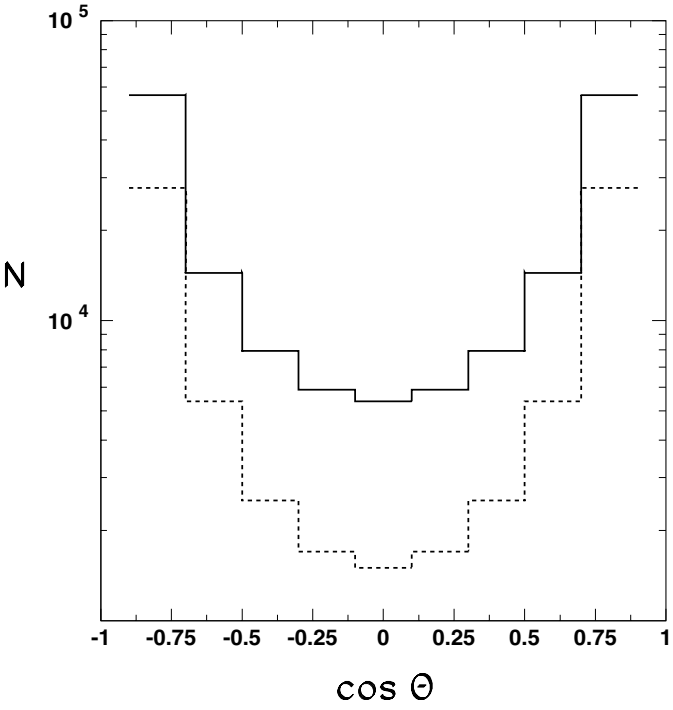

Fig. 4. Bin-integrated angular distributions of $N_{++}^{\rm bin}$ (solid line) and $N_{+-}^{\rm bin}$ (dashed line) in the SM at $\sqrt{s} = 500\,\text{GeV}$, $\mathcal{L}_{\rm int}(e^-e^-) = \mathcal{L}_{\rm int}(e^+e^-)/3$ with $\mathcal{L}_{\rm int}(e^+e^-) = 50\,\text{fb}^{-1}$ and $|P_1^-| = |P_2^-| = 0.8$

become smaller. The corresponding behavior of the statistical significance, defined as the ratio between deviations and uncertainties for each bin, are shown in Fig. 6, the analogue of Fig. 3.

We now proceed to the estimate of the constraints on the contact-interaction couplings from the two processes.

3 Numerical analysis and constraints on CI couplings

To assess the sensitivity of Bhabha and Møller scattering to the compositeness scale, we assume the data to be well-described by the SM predictions ($\epsilon_{ij} = 0$), i.e., that no deviation is observed within the foreseen experimental accuracy, and perform a χ^2 analysis of the $\cos\theta$ angular distribution. For each of the observable cross sections, the χ^2 distribution is defined as the sum over the above mentioned nine equal-size $\cos\theta$ bins introduced in Sect. 2:

$$\chi^2(\mathcal{O}) = \sum_{\rm bins} \left(\frac{\Delta(\mathcal{O})^{\rm bin}}{\delta\mathcal{O}^{\rm bin}} \right)^2 = \sum_{\rm bins} \left[\mathcal{S}(\mathcal{O})^{\rm bin} \right]^2 , \qquad (21)$$

where $\mathcal{O} = \sigma_{\rm L}$, $\sigma_{\rm R}$, $\sigma_{{\rm LR},t}$ and $\sigma^{\rm bin} \equiv \int_{\rm bin}(\mathrm{d}\sigma/\mathrm{d}z)\mathrm{d}z$. In (21), $\Delta(\mathcal{O})$ represents the relative deviation from the SM prediction defined in (13), and $\delta\mathcal{O}$ is the expected experimental relative uncertainty, that combines the statistical and the systematic one.

In order to achieve comparable accuracy in experimental measurements and theoretical predictions, radiative corrections to Bhabha and Møller scatterings have to be taken into account [23]. In practice, initial state radiation is by far the most relevant part of the QED modifications [24]. The method that we shall follow to evaluate the effects of the QED radiation for large-angle Bhabha scattering is the one that uses the so called structure function approach [24,25] where soft and hard photon emission is taken into account. As to Møller scattering, the QED corrections to the polarized cross section will be evaluated by means of the FORTRAN code MOLLERAD [26,27], adapted to the present discussion, with $m_{\rm top} = 175\,\text{GeV}$ and $m_H = 120\,\text{GeV}$.

Concerning the numerical inputs and assumptions used in the estimate of $\delta\mathcal{O}$, to assess the role of statistics we vary $\mathcal{L}_{\rm int}(e^+e^-)$ from 50 to $500\,\text{fb}^{-1}$. As for the systematic uncertainty, we take $\delta\mathcal{L}_{\rm int}/\mathcal{L}_{\rm int} = 0.5\%$, $\delta\epsilon/\epsilon = 0.5\%$ and, regarding the electron and positron degrees of polarization, $\delta P_1/P_1 = \delta P_2/P_2 = 0.5\%$.

As a criterion to constrain the values of the contact-interaction parameters allowed by the non-observation of the corresponding deviations, we impose $\chi^2 < \chi^2_{\rm CL}$, where the actual value of $\chi^2_{\rm CL}$ specifies the desired "confidence" level. We take the values $\chi^2_{\rm CL} = 3.84$ and 5.99 for 95% CL for a one- and a two-parameter fit, respectively.

3.1 Bhabha process

We begin the presentation of the numerical results from the consideration of $\sigma_{\rm L}$ and $\sigma_{\rm R}$. Since these cross sections simultaneously depend on the pairs of independent CI couplings $(\epsilon_{\rm LL}, \epsilon_{\rm LR})$ and $(\epsilon_{\rm RR}, \epsilon_{\rm LR})$ a two-parameter analysis is needed in these cases. The 95% CL allowed areas are represented by the elliptical contours around $\epsilon_{\rm LL} = \epsilon_{\rm RR} = \epsilon_{\rm LR} = 0$, depicted in Fig. 7a,b. The maximum reachable values of $\Lambda_{\rm RR}$ and $\Lambda_{\rm LL}$ correspond to the minimum of the lower branches of the curves in these figures.

Turning to $\epsilon_{\rm LR}$, the relevant cross section $\sigma_{{\rm LR},t}$ depends only on that parameter, see (7) and (8), so that the corresponding constraints are determined from a one-parameter fit (with the lower value of $\chi^2_{\rm CL}$). The model-independent, discovery reach expected at the Linear Collider for the corresponding mass scale $\Lambda_{\rm LR}$ is represented, as a function of the integrated luminosity $\mathcal{L}_{\rm int}$, in Fig. 8. In this figure, arrows indicate the planned luminosities collected at TESLA [4] and NLC [5]. As expected, the highest luminosity determines the strongest constraints on the CI couplings[4].

The 95% CL bounds on $\epsilon_{\rm LR}$ can be reported in Fig. 7a,b to narrow the constraints on $\epsilon_{\rm RR}$ and $\epsilon_{\rm LL}$, respectively. They are represented by the vertical lines there, so that the final allowed regions, at the 95% CL, are the shaded ones. Figure 8 dramatically shows the really high sensitivity of $\sigma_{{\rm LR},t}$, such that the discovery limits on $\Lambda_{\rm LR}$ are the highest, compared to the $\Lambda_{\rm RR}$ and $\Lambda_{\rm LL}$ case.

[4] Such increase with luminosity is somewhat slower than expected from the scaling law $\Lambda \sim (s\mathcal{L}_{\rm int})^{1/4}$ [28], since with

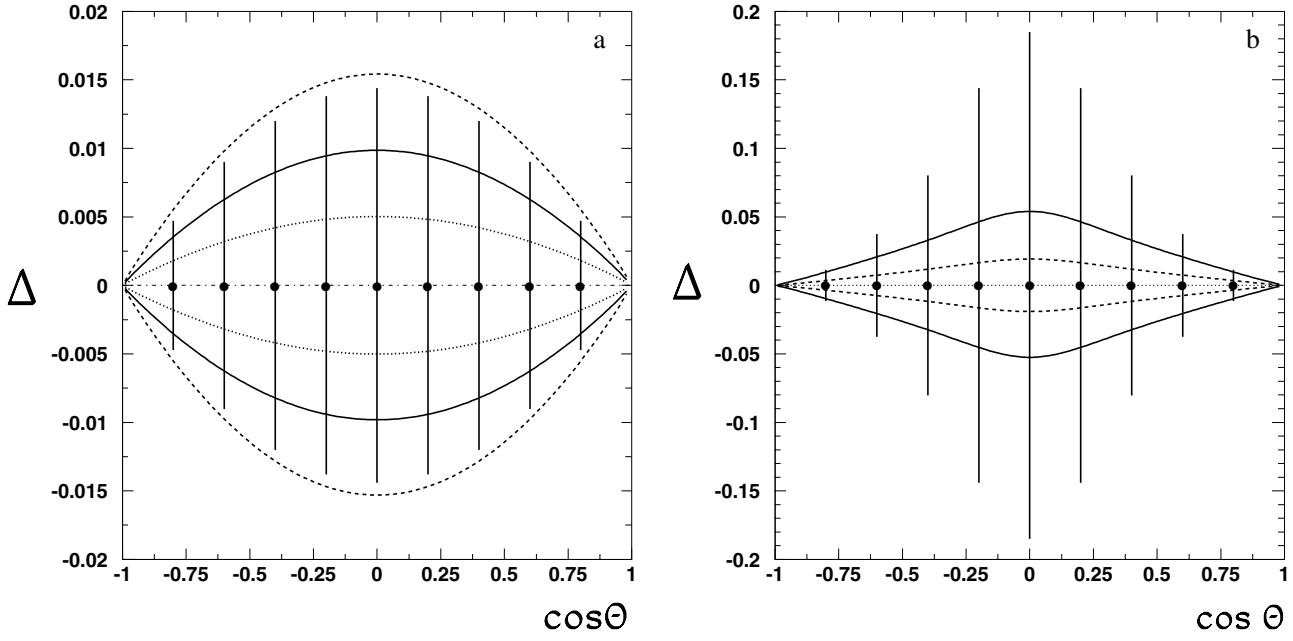

Fig. 5a,b. The angular distributions of relative deviations from SM predictions: **a** $\Delta(\sigma_{\rm RR})$ for $\Lambda_{\rm RR} = 40\,\text{TeV}$ (dashed line), 50 TeV (solid line) and 70 TeV (dotted line); **b** $\Delta(\sigma_{\rm LR})$ for $\Lambda_{\rm LR} = 30\,\text{TeV}$ (solid line) and 50 TeV (dashed line). The curves above (below) the horizontal line correspond to negative (positive) interference between contact-interaction and SM amplitude. The error bars show the expected statistical relevant uncertainty at $\mathcal{L}_{\rm int}(e^-e^-)$ to be the same as in Fig. 4

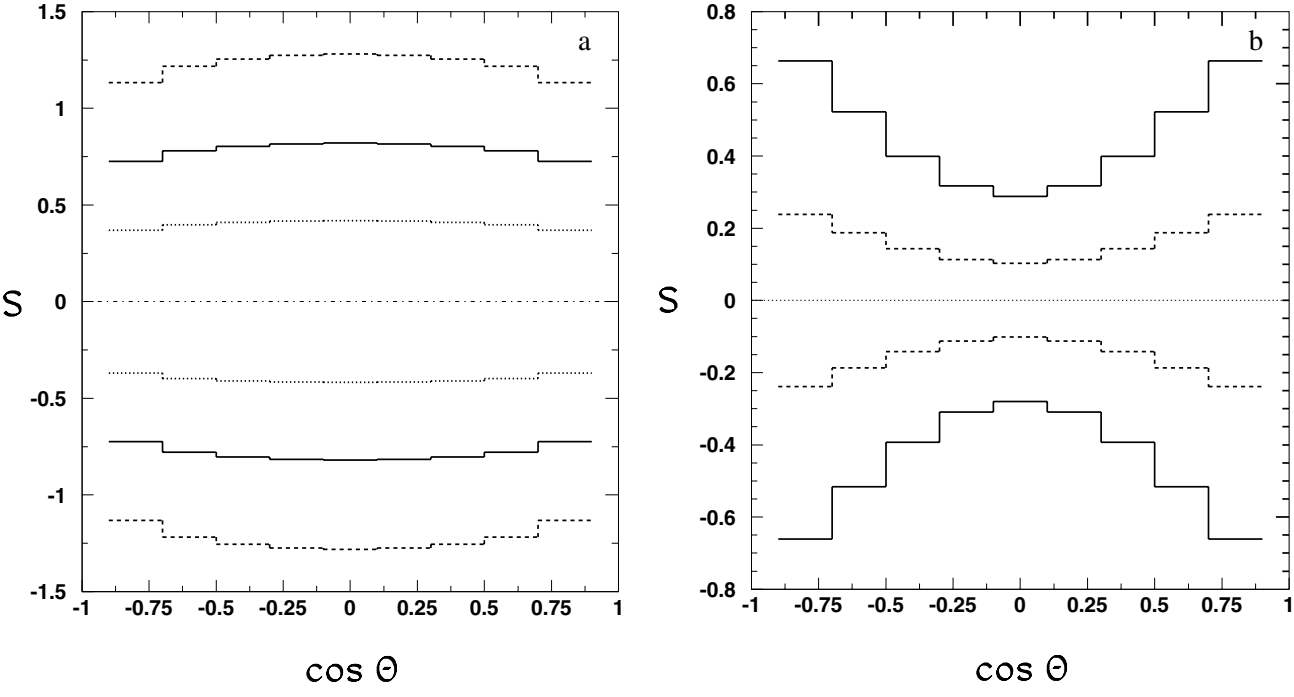

Fig. 6a,b. a Statistical significance $\mathcal{S}(\sigma_{\rm RR})$ as a function of $\cos\theta$ at $\Lambda_{\rm RR} = 40\,\text{TeV}$ (dashed line), 50 TeV (solid line) and 70 TeV (dotted line); **b** statistical significance $\mathcal{S}(\sigma_{\rm LR})$ as a function of $\cos\theta$ at $\Lambda_{\rm LR} = 30\,\text{TeV}$ (solid line) and 50 TeV (dashed line). Here, all inputs are the same as in Fig. 4

The crosses in Fig. 7a,b represent the model-dependent constraints obtainable by taking only one non-zero parameter at a time, instead of two simultaneously non-zero and independent as in the analysis presented above. The arms of the crosses refer to an integrated luminosity of $\mathcal{L}_{\rm int} = 50\,\text{fb}^{-1}$. One can note from Fig. 7a,b that the "single-parameter" constraints on the individual CI parameters

our input choice the effect of the systematic uncertainties can compete with the statistical one

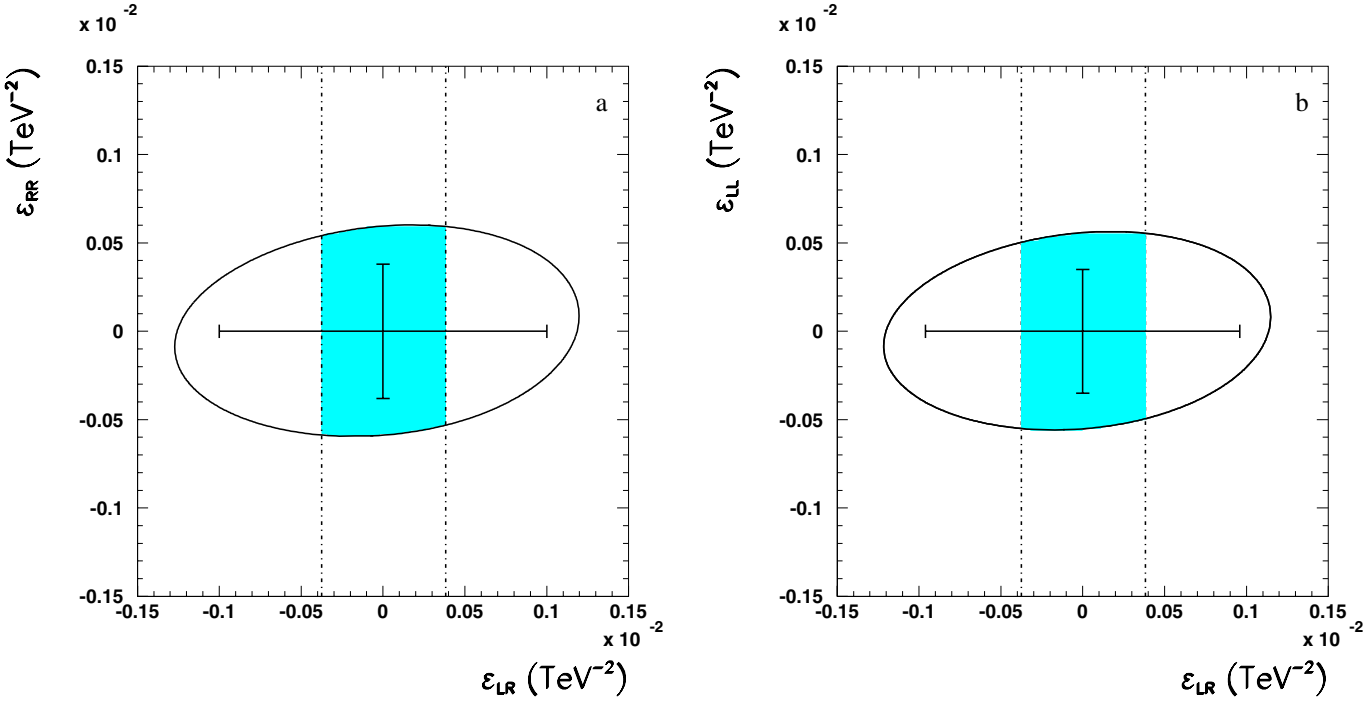

Fig. 7a,b. Allowed areas (ellipses) at 95% CL on electron contact-interaction parameters in the planes $(\epsilon_{\rm LR}, \epsilon_{\rm RR})$ and $(\epsilon_{\rm LR}, \epsilon_{\rm LL})$, obtained from $\sigma_{\rm R}$ **a** and $\sigma_{\rm L}$ **b**, respectively, at $\sqrt{s} = 500\,\text{GeV}$, $\mathcal{L}_{\rm int}(e^+e^-) = 50\,\text{fb}^{-1}$, $|P^-| = 0.8$ and $|P^+| = 0.6$. Vertical dashed curves indicate the allowed range for $\epsilon_{\rm LR}$ obtained from $\sigma_{{\rm LR},t}$

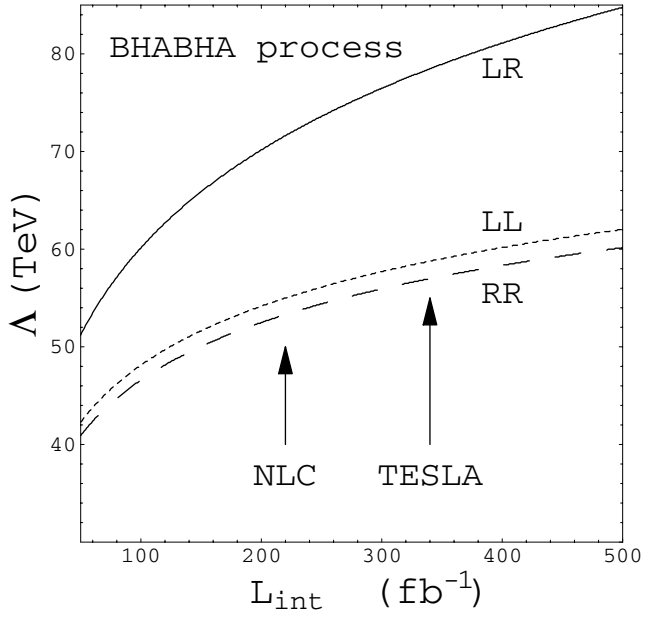

Fig. 8. Reach in Λ at 95% CL versus integrated luminosity $\mathcal{L}_{\rm int}(e^+e^-)$ obtained from the model-independent analysis for $e^+ + e^- \to e^+ + e^-$ at $E_{\rm c.m.} = 0.5\,\text{TeV}$, $|P^-| = 0.8$ and $|P^+| = 0.6$, $\Lambda_{\rm LR}$ (solid line), $\Lambda_{\rm RR}$ (dashed line), $\Lambda_{\rm LL}$ (dotted line). Arrows indicate the planned luminosities, $\mathcal{L}_{\rm int}(e^+e^-)$, at TESLA and NLC colliders

$\epsilon_{\rm RR}$ and $\epsilon_{\rm LL}$ are numerically more stringent, as compared to the model-independent ones. Essentially, this is a reflection of the smaller critical value of χ^2, $\chi^2_{\rm crit} = 3.84$, corresponding to 95% CL with a *one-parameter* fit.

3.2 Møller process

The procedure, and the criteria, to derive numerical constraints from the Møller process are quite similar, the outstanding difference being that, in this case, *each* measurable cross section in (18) depends on a single contact-interaction parameter, so that complete disentangling of the ϵ is directly obtained and the smaller $\chi^2_{\rm CL} = 3.84$, relevant to one-parameter cases, applies. Certainly, this is an advantage if one wants to perform a model-independent analysis of electron contact interactions. Also, a substantially higher longitudinal polarization should be attainable for electron beams than for positron ones, for a given luminosity. On the other side, there is the penalty of the lower luminosity expected in the e^-e^- mode, depressing the sensitivity. The lower bounds on the Λ are shown as a function of the integrated luminosity in Fig. 9.

4 Concluding remarks

In the previous sections we have derived limits on the electron contact interactions by simultaneously considering Bhabha scattering and Møller scattering at a Linear Collider with longitudinally polarized beams, using a model-independent analysis that allows one to simultaneously account for all independent couplings as non-vanishing free

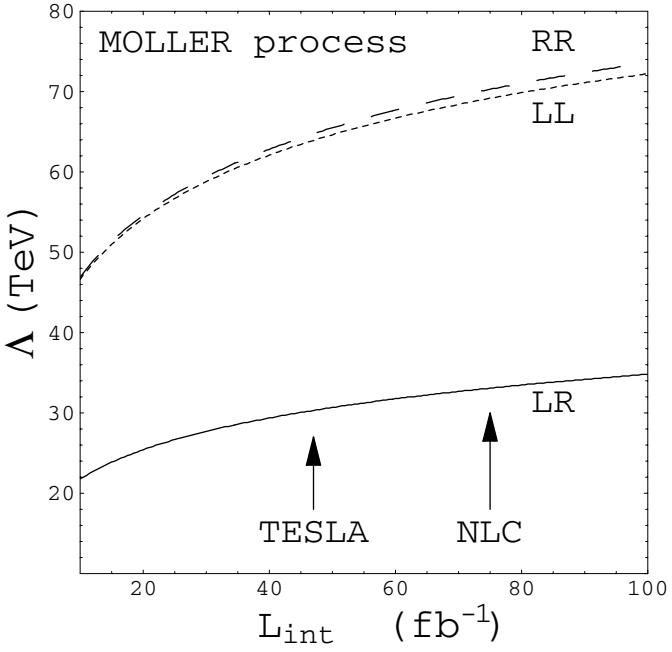

Fig. 9. Reach in Λ at 95% CL versus integrated luminosity $\mathcal{L}_{\rm int}(e^-e^-)$ obtained from the model-independent analysis for $e^- + e^- \to e^- + e^-$ at $E_{\rm c.m.} = 0.5\,\text{TeV}$, $|P_1^-| = |P_2^-| = 0.8$, $\Lambda_{\rm LR}$ (solid line), $\Lambda_{\rm RR}$ (dashed line), $\Lambda_{\rm LL}$ (dotted line). Arrows indicate the planned luminosities, $\mathcal{L}_{\rm int}(e^-e^-)$, at TESLA and NLC colliders

parameters. The analysis is based on the definition of measurable polarized differential cross sections that allows one to derive

(i) from Bhabha scattering, separate bounds on $\epsilon_{\rm LR}$ and in the planes $(\epsilon_{\rm LL}, \epsilon_{\rm LR})$ and $(\epsilon_{\rm RR}, \epsilon_{\rm LR})$;
(ii) from Møller scattering, completely individual bounds on $\epsilon_{\rm LL}$, $\epsilon_{\rm RR}$ and $\epsilon_{\rm LR}$.

Numerical results for the lower bounds on the corresponding range in the relevant mass scales Λ_{ij}, depending on the luminosity, are shown in Figs. 8 and 9, and are summarized in Table 1 specifically for the potential of TESLA and NLC to search for four-lepton contact interactions. One may conclude from the results reported in Table 1 that the two processes can be complementary as far as the sensitivity to the individual couplings in a model-independent data analysis is concerned: the sensitivity of Bhabha scattering to $\Lambda_{\rm LR}$ is dramatically higher, while Møller scattering should be the one most sensitive to $\Lambda_{\rm LL}$ and $\Lambda_{\rm RR}$, provided the luminosity in this running mode does not fall below the planned values.

All this shows the benefits of initial beam longitudinal polarization, that allows one, by measuring suitable combinations of polarized cross sections, to directly disentangle the individual couplings. Indeed, as previously observed, in general without polarization only correlations among contact-interaction parameters, rather than finite allowed regions, could be derived and, consequently, in the unpolarized case only a one-parameter analysis, relating to a specific model, can be performed.

Table 1. Reach in Λ_{ij} at 95% CL, achievable at TESLA and NLC and from the model-independent analysis performed for $e^+e^- \to e^+e^-$ and $e^-e^- \to e^-e^-$. $\sqrt{s} = 0.5\,\text{TeV}$, $|P^-| = 0.8$ and $|P^+| = 0.6$

Process	$\mathcal{L}_{\rm int}$ fb^{-1}	$\Lambda_{\rm LL}$ TeV	$\Lambda_{\rm RR}$ TeV	$\Lambda_{\rm LR}$ TeV
	TESLA: 340	59	57	79
$e^+e^- \to e^+e^-$	NLC: 220	55	54	72
	TESLA: 47	64	65	30
$e^-e^- \to e^-e^-$	NLC: 75	69	70	33

Acknowledgements. This research has been partially supported by MIUR (Italian Ministry of University and Research) and by funds of the University of Trieste.

References

1. See, e.g. G. Pasztor, M. Perelstein, SNOWMASS-2001-P315, November 2001, hep-ph/0111471; S. Cullen, M. Perelstein, M. Peskin, Phys. Rev. D **62**, 055012 (2000)
2. T.G. Rizzo, SLAC-PUB-9295, hep-ph/0208027
3. E. Eichten, K. Lane, M.E. Peskin, Phys. Rev. Lett. **50**, 811 (1983); R. Rückl, Phys. Lett. B **129**, 363 (1983)
4. TESLA Technical design report, Pt. 2, edited by R. Brinkmann, K. Flottmann, J. Rossbach, P. Schmuser, N. Walker, H. Weise, DESY-01-011 (2001)
5. Linear collider physics resource book for Snowmass 2001, T. Abe et al., SLAC-R-570
6. Proceedings of the Electron-Electron Linear Collider Workshop, December 1999, Santa Cruz (CA), edited by C.A. Heusch, Int. J. Mod. Phys. A **15**, No. 16, (2000)
7. C. Geweniger et al., Combination of the LEP II $f\bar{f}$ Results, LEP2FF/01-02 (2001)
8. D. Bourilkov, Phys. Rev. D **64**, 071701 (2001)
9. K. Cheung, Phys. Lett. B **517**, 167 (2001); V. Barger, K. Cheung, Phys. Lett. B **480**, 149 (2000), and references therein
10. A.F. Zarnecki, Nucl. Phys. Proc. Suppl. **79**, 158 (1999)
11. A.A. Babich, P. Osland, A.A. Pankov, N. Paver, LC Note LC-TH-2001-021 (2001), hep-ph/0101150; Phys. Lett. B **518**, 128 (2001)
12. B. Schrempp, F. Schrempp, N. Wermes, D. Zeppenfeld, Nucl. Phys. B **296**, 1 (1988)
13. D. Bardin, W. Hollik, T. Riemann, Z. Phys. C **49**, 485 (1991)
14. E.J. Eichten, S. Keller, in Physics at the First Muon Collider, November 1977, Batavia, IL, hep-ph/9801258
15. M. Beccaria, F.M. Renard, S. Spagnolo, C. Verzegnassi, Phys. Rev. D **62**, 053003 (2000)
16. For earlier discussions of polarization in the processes (1) and (2) see, e.g.: R. Gastmans, Y. Van Ham, Phys. Rev. D **10**, 3629 (1974); L.L. Deraad, Phys. Rev. D **11**, 3328 (1975); M.J. Puhala, T.G. Rizzo, B.L. Young, Phys. Lett. B **109**, 411 (1982); H.A. Olsen, P. Osland, Phys. Rev. D **25**, 2895 (1982); S. Jadach, B.F.L. Ward, Phys. Rev. D **54**, 743 (1996), and references therein
17. M. Consoli, W. Hollik, F. Jegerlehner, CERN-TH-5527-89, presented at the Workshop on Z Physics at LEP

18. G. Altarelli, R. Casalbuoni, D. Dominici, F. Feruglio, R. Gatto, Nucl. Phys. B **342**, 15 (1990)
19. F. Cuypers, PSI-PR-96-32, hep-ph/9611336, in New directions in high-energy physics, edited by D.G. Cassel, L. Trindle Gennari, R.H. Siemann, p. 878
20. F. Cuypers, P. Gambino, Phys. Lett. B **388**, 211 (1996)
21. A. Czarnecki, W.J. Marciano, Int. J. Mod. Phys. A **15**, 2365 (2000); Phys. Rev. D **53**, 1066 (1996)
22. J.E. Spencer, Int. J. Mod. Phys. A **11**, 1675 (1996)
23. A. Denner, S. Pozzorini, Eur. Phys. J. C **7**, 185 (1999); M. Bohm, A. Denner, W. Hollik, Nucl. Phys. B **304**, 687 (1988)
24. O. Nicrosini, L. Trentadue, in Radiative Corrections for e^+e^- Collisions, edited by J.H. Kühn (Springer, Berlin, 1989), p. 25; O. Nicrosini, L. Trentadue, in QED Structure Functions, edited by G. Bonvicini, AIP Conf. Proceedings No. 201 (AIP, New York 1990), p. 12
25. G. Montagna, O. Nicrosini, F. Piccinini, Phys. Rev. D **48**, 1021 (1993)
26. V.A. Mosolov, N.M. Shumeiko, J.G. Suarez, see [6], Int. J. Mod. Phys. A **15**, 2377 (2000)
27. N.M. Shumeiko, J.G. Suarez, J. Phys. G **26**, 113 (2000)
28. T.L. Barklow, Int. J. Mod. Phys. A **11**, 1579 (1996)